



## ORIGINAL ARTICLE

# Synthesis and study on aroylhydrazones having cyanovinylpyrrole



Poonam Rawat, R.N. Singh \*

Department of Chemistry, University of Lucknow, Lucknow 226007, U.P., India

Received 3 January 2015; accepted 8 March 2015

Available online 16 March 2015

## KEYWORDS

Emission;  
TD-DFT;  
NBO;  
First hyperpolarizabilities

**Abstract** A series of *C*-cyanovinylpyrrole containing aroylhydrazones (**3a–c**), derived from ethyl 2-cyano-3-(5-formyl-1*H*-pyrrol-2-yl)-acrylate and acid hydrazides: salicylhydrazide, isoniazid and 3,5-dinitrobenzohydrazide have been characterized by various spectroscopic techniques (<sup>1</sup>H NMR, <sup>13</sup>C NMR, Mass, UV–Visible, Emission, FT-IR) and quantum chemical calculations. TD-DFT has been used to calculate the various electronic excitations and their nature. The emission spectra show that (**3a–c**) are good photoluminescent material due to intense emission at higher wavelength in yellow, green and blue region with high Stoke's shift in the region 80–328 nm. The molar refractivity (*MR*) for (**3a–c**) is calculated as 109.28, 102.96, 119.14 esu, respectively. Natural bond orbital (NBO) analysis has been carried out to explore the various conjugative and hyperconjugative interactions within molecule and their second order stabilization energy (*E*<sup>(2)</sup>). Global electrophilicity index ( $\omega = 5.41\text{--}8.11$  eV) shows that (**3a–c**) molecules work as strong electrophiles. The local reactivity descriptors analyses such as Fukui functions ( $f_k^+$ ,  $f_k^-$ ), local softnesses ( $s_k^+$ ,  $s_k^-$ ) and electrophilicity indices ( $\omega_k^+$ ,  $\omega_k^-$ ) have been performed to determine the reactive sites within molecules. The first hyperpolarizabilities ( $\beta_0$ ) of (**3a–c**) have been computed and found to increase with electron withdrawing substituents.

© 2015 The Authors. Published by Elsevier B.V. on behalf of King Saud University. This is an open access article under the CC BY-NC-ND license (<http://creativecommons.org/licenses/by-nc-nd/4.0/>).

## 1. Introduction

Aroylhydrazones ( $\text{>C=N-NH-CO-}$ ) are special group of compounds in the Schiff bases family that have wide applications in chemistry and biology and are characterized by the

\* Corresponding author. Tel.: +91 9451308205.

E-mail address: [rnsvk.chemistry@gmail.com](mailto:rnsvk.chemistry@gmail.com) (R.N. Singh).

Peer review under responsibility of King Saud University.



Production and hosting by Elsevier

presence of two inter-linked nitrogen atoms as  $\text{Nsp}^2\text{--Nsp}^3$ . They are good synthons for the target syntheses of 1,3,4-oxadiazine, 1,2,4-triazine, pyrazole derivatives (Mohareb et al., 2010) and 1,3,4-oxadiazolines, 2-azetidinones, 4-thiazolidinones via heterocyclic transformations (Rollas and Küçükgülzel, 2007; Armbruster et al., 2006). Several aroylhydrazones have wide applications in the field of analytical chemistry as a selective metal extracting agent as well as in spectrophotometric determination of certain transition metals (Tang et al., 2004; Kavlentis, 1998; Chalapathi et al., 2011). However, the most valuable property of aroylhydrazones is their great physiological activity due to the presence of the active pharmacophore ( $\text{>C=N-NH-CO-}$ ) and provides a

wide range of application in medicinal and pharmaceutical fields with various biological applications. Therefore, a number of hydrazone derivatives have been used for the treatment of diseases such as convulsant (Dimmock et al., 2000), malaria (Melnyk et al., 2006), HIV, cancer (Savini et al., 2004), microbial (Rallas et al., 2002; Gursoy et al., 1997; Ajani et al., 2010; Rawat and Singh, 2014a, 2014b, 2015a, 2015b) and tuberculosis (Zheng et al., 2009; Richardson and Bernhardt, 1999; Bedia et al., 2006; Darnell and Richardson, 1999; Murukan and Mohanan, 2007). Many of hydrazones are used as prospective new materials for the development of potential chemosensors (Yu et al., 2007), opto-electronic (Szczesna and Lipkowska, 2001) and nonlinear optical (NLO) (Vijayakumar et al., 2010, 2011; Shirota and Kageyama, 2007; Blau, 1987; Vogt et al., 2008; Genger et al., 2008) applications.

The functionalized *C*-vinylpyrroles are prospective new materials for molecular optical switches, nano-devices, photo- and electro-conducting applications and also used as ligands for new photo catalysts, biologically active complexes (Hayes et al., 2000; Harmjanz et al., 2000; Sour et al., 1999). Therefore, the title compounds (**3a–c**) have been synthesized and characterized using various experimental and theoretical spectroscopic methods. In present paper, we report the spectroscopic, structural and NLO properties of these molecules. Furthermore, quantum chemical calculations have also been performed to determine the intramolecular conjugative and hyperconjugative interactions, hydrogen bonding, chemical reactivity and NLO properties of investigated molecules.

## 2. Experimental details

All the chemicals were used of analytical grade. The pyridine-4-carboxylic acid hydrazide or isoniazid was purchased from sigma Aldrich company. Ethyl 2-cyano-3-(5-formyl-1*H*-pyrrol-2-yl)-acrylate (**1**) was prepared by an earlier reported method (Kjell and Per-Åke, 1979). The salicylhydrazide and 3,5-dinitrobenzohydrazide (**2a**, **2c**) were prepared according to the literature procedure (Gup and Kirkan, 2005; Wild, 1947). All spectra were recorded at 25 °C. The Mass spectra of (**3a–c**) were recorded on JEOL-Acc TDF JMS-T100LC, Accu TOF mass spectrometer. The <sup>1</sup>H NMR spectra of (**3a–c**) were recorded in DMSO-*d*<sub>6</sub> on Bruker DRX-300 spectrometer using TMS as an internal reference. The <sup>13</sup>C NMR spectra of (**3a–c**) were recorded in DMSO-*d*<sub>6</sub> on Bruker DRX-300 spectrometer using TMS as an internal reference. The FT-IR spectra were recorded in KBr medium on a Bruker spectrometer. The UV–Visible absorption spectra of (**3a–c**), (1 × 10<sup>−5</sup> M in DMSO) were recorded on V-670 JASCO spectrophotometer. The emission spectra of (**3a–c**), (1 × 10<sup>−5</sup> M in DMSO) were recorded on PL Spectrometer LS-55, Perkin Elmer, UK.

### 2.1. Preparation of ethyl 3,5-dinitrobenzoate (Vogel, 1956)

3,5-dinitrobenzoic acid (5.320 g) was dissolved in 15 ml ethanol and 1.0 ml of conc. H<sub>2</sub>SO<sub>4</sub> was added as catalyst and solution was refluxed for 20 h. The solution was cooled down to room temperature and refrigerated for 8 h to precipitation. The precipitate was recrystallized in ethanol to give the product ethyl 3,5-dinitrobenzoate. m.p. – 90 °C.

### 2.2. Preparation of 3,5-dinitrobenzohydrazide (Wild, 1947)

Ethyl 3,5-dinitrobenzoate (1.60 g, 6.6633 mmol) and hydrazine hydrate (0.48 ml, 0.01 mol) of 100% in 10 ml of methanol were refluxed for 10 h. The solution was cooled to room temperature to obtain yellow colored precipitate. The precipitate was filtered off and recrystallized from methanol to give pure product 3,5-dinitrobenzohydrazide.

Color: dark yellow, yield: (0.9422 g, 62.54%), m.p.: 145 °C.

### 2.3. Preparation of 2-hydroxybenzohydrazide (salicylhydrazide) (Gup and Kirkan, 2005)

A solution of hydrazine hydrate (0.1645 g, 0.16 ml, 3.286 mmol) in 10 ml methanol was added dropwise to the stirring solution of methyl 2-hydroxybenzoate (0.500 g, 0.42 ml, 3.286 mmol) in 25 ml methanol. Reaction mixture was refluxed for 6 h. After refluxing, cream color precipitate was obtained. The precipitate was filtered off, washed with methanol and dried in air.

Color: creamy white, yield: 0.3020 g, 72.88%, m.p.: 140 °C.

### 2.4. Ethyl 2-cyano-3-[5-((2-hydroxy-benzoyl)-hydrazonomethyl)-1*H*-pyrrol-2-yl]-acrylate (**3a**)

To the equimolar solution of ethyl 2-cyano-3-(5-formyl-1*H*-pyrrol-2-yl)-acrylate (**1**) (0.200 g, 0.9171 mmol) and 2-hydroxy-benzoic acid hydrazide (**2a**) (0.1394 g, 0.9171 mmol) in 20 ml methanol, 0.01 ml of conc. HCl acid was added as catalyst. The reaction mixture was stirred at room temperature for overnight to obtain yellow color precipitate. The precipitate was filtered off, washed with MeOH and dried in air, afforded (**3a**), as dark yellow solid. Yield: 0.1582 g, 48.96%. M.p.: 278–280 °C. Anal. calcd. for C<sub>18</sub>H<sub>16</sub>N<sub>4</sub>O<sub>4</sub>: C 61.34%, H 4.57%, N 15.90%; obs.: C 61.38%, H 4.54%, N 15.92%. MS (*m/z*): calcd. 352.1171, obs. 353 [M<sup>+</sup> + 1]. <sup>1</sup>H NMR (300 MHz, DMSO-*d*<sub>6</sub>) δexp/calcd 12.680/12.545 (s, 1H, –OH), δ 12.050/10.313 (s, 1H, pyrrole-NH), 12.039/9.582 (s, 1H, ArCONH), 8.367/8.085 (s, 1H, vinyl-CH=C), 7.850–7.876/7.872–7.169 (d, *J* = 7.8 Hz, 2H, Ar-CH), 6.953–6.980/7.872–7.169 (t, *J* = 9.75 Hz, 2H, Ar-CH), 7.407/7.97 (s, 1H, –CH=N), 7.444–7.457, 6.887–6.875/6.966–7.253 (m, 2H, *J* = 3.9, 3.6 Hz, pyrrole-CH), 4.231–4.301/4.347 (q, *J* = 7.00 Hz, 2H, ester-CH<sub>2</sub>), 1.263–1.310/1.473–1.236 (t, *J* = 7.05 Hz, 3H, ester-CH<sub>3</sub>). <sup>13</sup>C NMR (300 MHz, DMSO-*d*<sub>6</sub>) δexp/calcd C2-123.22/128.08, C3-122.26/126.82, C4-113.98/115.7, C5-132.39/137.05, C6-141.95/141.44, C7-108.27/91.89, C8-114.34/116.08, C10-163.68/161.23, C13-50.28/65.16, C14-15.23/16.72, C15-145.38/132.42, C18-168.54/162.88, C20-111.29/112.53, C21-120.42/124.33, C22-120.42/116.25, C23-129.53/133.29, C24-129.53/115.99, C25-158.48/160.96.

### 2.5. Synthesis of ethyl 2-cyano-3-[5-((4-nitro-benzoyl)-hydrazonomethyl)-1*H*-pyrrol-2-yl]-acrylate (**3b**)

To the equimolar solution of ethyl 2-cyano-3-(5-formyl-1*H*-pyrrol-2-yl)-acrylate (0.250 g, 1.1464 mmol) and isoniazid (0.1572 g, 1.1464 mmol) in 25 ml methanol, 0.01 ml of conc. HCl acid was added as catalyst. The reaction mixture was stirred at room temperature for 8 h and yellow color precipitate

was obtained. The precipitate was filtered off, washed with methanol and dried in air, afforded (**3b**), as yellow solid. Yield: 0.3464 g, 89.63%. The compound decomposes above 280 °C. Anal. calcd. for C<sub>17</sub>H<sub>15</sub>N<sub>5</sub>O<sub>3</sub>: C 60.51%, H 4.48%, N 20.76%; obs.: C 60.54%, H 4.50%, N 20.72%. MS (*m/z*): calcd. 337.117; obs. 338.14 [M<sup>+</sup> + 1]. <sup>1</sup>H NMR (300 MHz, DMSO-*d*<sub>6</sub>) δ<sub>exp</sub>/calcd 12.749/10.3155 (s, 1H, pyrrole-NH), 12.707/9.5591 (s, 1H, ArCONH), 8.790/8.0801 (s, 1H, vinyl-CH=C), 8.369–8.343/9.0865–9.1345 (d, *J* = 7.8 Hz, 2H, pyridine-CH), 8.463/7.9717 (s, 1H, —CH=N—), 6.974–6.995/7.8626–8.1343 (d, *J* = 6.3 Hz, 2H, pyridine-CH), 6.779–6.769/7.2548 (d, 2H, *J* = 3.6, 2.7 Hz, pyrrole-CH), 8.596–8.587/6.9616 (d, *J* = 2.7 Hz, 1H, pyrrole-CH), 4.247–4.314/4.3452–4.3542 (q, *J* = 6.70 Hz, 2H, ester-CH<sub>2</sub>), 1.283–1.243/1.2348–1.4826 (t, *J* = 6.0 Hz, 3H, ester-CH<sub>3</sub>). <sup>13</sup>C NMR (300 MHz, DMSO-*d*<sub>6</sub>) δ<sub>exp</sub>/calcd C2-125.24/128.1798, C3-123.60/126.8273, C4-116.96/115.9032, C5-133.84/136.9796, C6-138.68/141.5059, C7-114.98/92.0105, C8-113.94/116.0699, C10-157.56/161.2264, C13-52.20/65.1485, C14-15.28/16.6665, C15-141.82/132.6996, C18-159.92/158.5427, C20-129.78/139.4344, C21-117.68/118.2875, C22-142.67/148.5444, C24-142.67/148.8017, C25-117.68/122.2078.

#### 2.6. Synthesis of ethyl 2-cyano-3-[5-[(3,5-dinitro-benzoyl)-hydrazonomethyl]-1H-pyrrol-2-yl]-acrylate (**3c**)

To the equimolar solution of ethyl 2-cyano-3-(5-formyl-1H-pyrrol-2-yl)-acrylate (**1**) (0.250 g, 1.1464 mmol) and 3,5-dinitro-benzohydrazide (**2c**) (0.2592 g, 1.1464 mmol) in 25 ml methanol, 0.01 ml of conc. HCl acid was added as catalyst. The reaction mixture was stirred at room temperature. After stirring for 4 h, dark yellow color precipitate was obtained. The precipitate was filtered off, washed with methanol and dried in air, afforded (**3c**), as yellow solid. Yield: 0.3844 g, 78.68%. Anal. calcd. for C<sub>18</sub>H<sub>14</sub>N<sub>6</sub>O<sub>7</sub>: C 50.69%, H 3.31%, N 19.71%; obs.: C 50.72%, H 3.28%, N 19.74%. MS (*m/z*): calcd. 426.0924; obs. 427.18 [M<sup>+</sup> + 1]. <sup>1</sup>H NMR (300 MHz, DMSO-*d*<sub>6</sub>) δ<sub>exp</sub>/calcd 12.675/10.4148, (s, 1H, pyrrole-NH), 12.110/9.0539, (s, 1H, ArCONH), 8.366/9.4455, (s, 1H, Ar-CH), 7.867/9.3966, (s, 1H, Ar-CH), 7.566/9.0367, (s, 1H, Ar-CH), 7.496/7.9468, (s, 1H, vinyl-CH=C), 7.447/7.8184, (s, 1H, —CH=N—), 6.877/7.0459, (s, 1H, pyrrole-CH), 6.127/6.8171, (s, 1H, pyrrole-CH), 4.230–4.299/4.3266–4.3243, (q, *J* = 6.90 Hz, 2H, ester-CH<sub>2</sub>), 1.263–1.310/1.2642–1.4851, (t, *J* = 7.05 Hz, 3H, ester-CH<sub>3</sub>). <sup>13</sup>C NMR (300 MHz, DMSO-*d*<sub>6</sub>) δ<sub>exp</sub>/calcd C2-126.04/128.6533, C3-122.58/126.153, C4-117.98/116.3081, C5-133.04/135.7931, C6-138.96/141.43, C7-116.64/93.2815, C8-113.89/115.4622, C10-158.74/160.6803, C13-53.03/65.6575, C14-15.94/16.7965, C15-144.05/133.6347, C18-157.66/155.1949, C31-128.88/136.2025, C32-127.15/130.9513, C33-139.64/148.7423, C34-119.57/122.1914, C35-139.64/147.9564, C36-127.15/125.8432.

### 3. Quantum chemical calculations

The quantum chemical calculations have been carried out using Gaussian 09 program package (Frisch et al., 2010) to predict the optimized geometry of molecular structure, <sup>1</sup>H NMR chemical shifts, vibrational wave numbers, global and local reactivity descriptors, first hyperpolarizability at B3LYP functional and 6-31G(d,p) basis set. To estimate the

thermodynamic parameters as enthalpy (*H*) and Gibbs free energy (*G*), the thermal corrections to these parameters are added to the calculated total energies. The <sup>1</sup>H NMR chemical shifts are calculated using gauge including atomic orbital (GIAO) approach using IEFPCM model in appropriate solvent. Time dependent density functional theory (TD-DFT) is used to find the various electronic excitations and their nature within molecule. The optimized geometrical parameters are used in the vibrational wave numbers calculation to characterize all stationary points as minima and their harmonic vibrational wave numbers are positive. Gauss-View program is used for visualization of optimized geometry of molecule (Gauss-View).

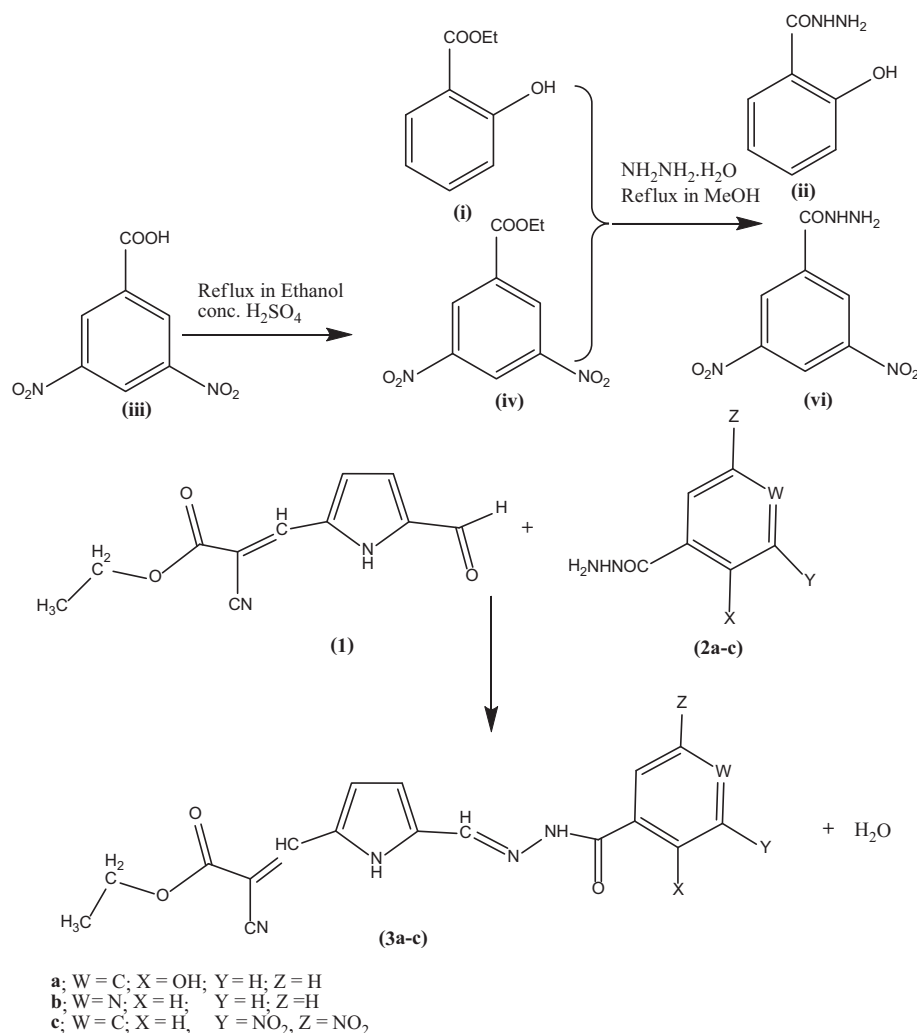
### 4. Results and discussion

#### 4.1. Molecular geometry and stability of conformers

The route for the formation of products (**3a–c**) involved in chemical reactions is shown in Scheme 1. The optimized geometry for the ground state lower energy conformer of (**3a–c**) is shown in Fig. 1. Selected optimized geometrical parameters of (**3a–c**), calculated at B3LYP/6-31G(d,p) are listed in Supplementary material (S Table 1). The ground state lower energy conformer of all the molecules (**3a–c**) possesses C<sub>1</sub> symmetry. The asymmetry of the N1–C2 and N1–C5 bonds *i.e.* difference between their bond lengths can be explained due to the presence of the two different groups as 'ethyl 2-cyano-acrylate' and 'aroyl hydrazonomethyl' at C2, C5 of pyrrole ring, respectively. The *E*-configuration about the vinyl C6=C7 bond with respect to the higher priority group ethoxycarbonyl and pyrrole gives lower energy conformer. The molecule also exists in *E*-configuration with respect to the pyrrole and —NH—CO—Ar group located on the opposite side of the Schiff base C15=N16 bond. The *E*-configuration about Schiff base C15=N16 bond is not only observed in our theoretical study but also reported in crystal structure of various aroylhydrazone derivatives (Wei, 2012; Zong, 2012). In (**3a–c**), due to the presence of intramolecular hydrogen bonding (N1–H27/26/20···N9) the pyrrole N–H bond is elongated than free N–H bond (Rawat and Singh, 2014a, 2014b, 2014c, 2015a, 2015b; Singh et al., 2013a, 2013b, 2013c, 2013e, 2014a, 2014b).

#### 4.2. <sup>1</sup>H and <sup>13</sup>C NMR spectroscopy

NMR calculations are now attainable and accurate enough to be useful exploring the relationship between chemical shift and molecular structure. Density functional theory (DFT) has emerged in recent years as a promising alternative to conventional *ab initio* methods in quantum chemistry. It therefore seems reasonable to investigate in detail how well DFT predicts magnetic response properties, in particular shielding tensors (Kim et al., 2000). A number of methods have been developed for the calculation of molecular second-order magnetic response properties. It is generally accepted that accurate prediction of these properties within the finite basis approximation, requires gauge-invariant procedures (Wolinski et al., 1990). The geometry of (**3a–c**) compounds, together with that of tetramethylsilane (TMS) is fully optimized. <sup>1</sup>H and <sup>13</sup>C NMR chemical shifts are calculated with GIAO approach at



**Scheme 1** Optimized geometry of the reactants (1, 2a-c) and products (3a-c).

B3LYP/6-31G(d,p) method. The experimental <sup>1</sup>H NMR spectra of products (3a-c) in DMSO-*d*<sub>6</sub> are given in [Supplementary Fig. S1a-c](#). The <sup>1</sup>H NMR chemical shifts (δ/ppm) of (3a-c) are assigned in Sections 2.4-2.6. In the <sup>1</sup>H NMR spectra of (3a-c), a quartet and a triplet chemical shift designate the presence of ester -CH<sub>2</sub>, -CH<sub>3</sub> group in all the molecules. In (3a-c), the observed chemical shifts as a singlet at 7.404, 8.463, 7.447 ppm indicate presence of the hydrazone linkage (CH=N-NH-) in these molecules. The big difference in the certain experimental and calculated chemical shift of the compound is due to the formation of intermolecular hydrogen bonding with solvent. The pyrrolic NH and hydrazone NH appear at downfield in experimental spectra due to the formation of intermolecular hydrogen bonding with DMSO solvent. The higher chemical shift for ArCONH is observed due to intermolecular hydrogen bonding with solvent than calculated in gaseous state. In order to compare the chemical shifts, correlation graph between the experimental and calculated <sup>1</sup>H NMR chemical shifts is shown in [Supplementary Fig. S2](#). The correlation coefficients ( $R^2 = 0.937, 0.893, 0.927$ ) for (3a-c), show that experimental <sup>1</sup>H NMR data are consistent

with the calculated data from optimized structure of probed molecules.

The experimental <sup>13</sup>C NMR spectra of (3a-c) in DMSO-*d*<sub>6</sub> are given in [Supplementary Fig. S3a-c](#). Additional support for molecular structures of (3a-c) is provided by their <sup>13</sup>C NMR spectra, in which chemical shifts of the C15 carbon atom at 145.38, 143.39, 144.05 ppm for -CH=N-NH and C18 carbon atom at 168.54, 160.46, 157.66 ppm for -NH-CO-Ar confirm the aroylhydrazone character of these molecules. In order to compare the chemical shifts, correlation graph between the experimental and calculated <sup>13</sup>C NMR chemical shifts is shown in [Supplementary Fig. S4](#). The correlation coefficients ( $R^2 = 0.937, 0.952, 0.967$ ) show that there is a good agreement between experimental and calculated <sup>13</sup>C NMR chemical shifts.

The mass spectra of (3a-c) showed [*M* + 1] peaks with agreement of their molecular formula. The molecular ion *M* + 1 peaks observed at *m/z*: 353, 338 and 427 corresponding to their relative molecular mass peaks in 3a, 3b and 3c, mass spectra respectively are shown in [Supplementary material Fig. S5a-c](#).

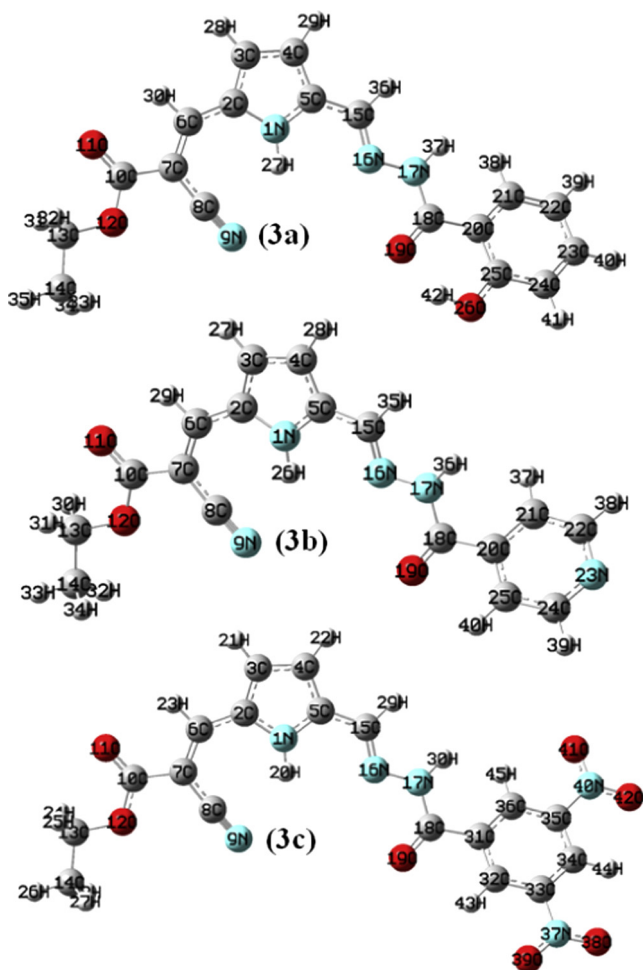


**Figure 1** Optimized geometry for the ground state lower energy conformer of (3a-c).

#### 4.3. Electronic absorption (UV-Visible) and natural bond orbitals (NBO) analysis

The nature of excitations in the observed UV-Visible spectra of (3a-c) compounds has been studied by the time dependent density functional theory (TD-DFT). The calculated and experimental electronic excitations of high oscillatory strength are listed in Table 1. The experimental UV-Visible spectra of (3a-c) are shown in Fig. 2 and molecular orbital plots are shown in Supplementary material Fig. S6. The vicinal orbitals

**Table 1** Comparison between calculated and experimental electronic excitations for (3a-c):  $E/eV$ , oscillatory strength ( $f$ ), ( $\lambda_{\max}/nm$ ) at TD-DFT/B3LYP/6-31G(d,p) level.

Excitations	E (eV)	( $f$ )	$\lambda$ calcd.	$\lambda$ obs.	Assignment	
(3a)	H-2 $\rightarrow$ L	4.1973	0.1662	295.39	244	$\pi \rightarrow \pi^*$
	H $\rightarrow$ L	2.9078	0.9548	426.38	412	$\pi \rightarrow \pi^*$
(3b)	H $\rightarrow$ L + 2	4.9148	0.4711	252.27	233	$n \rightarrow \pi^*$
	H $\rightarrow$ L	2.980	0.9518	416.01	389	$n \rightarrow \pi^*$
(3c)	H-6 $\rightarrow$ L + 1	4.910	0.5936	252.47	242	$\pi \rightarrow \pi^*$
	H $\rightarrow$ L + 2	3.002	0.8984	413.00	402	$n \rightarrow \pi^*$

of HOMO and LUMO play the same role of electron donor and electron acceptor, respectively. The HOMO-LUMO energy gap is an important reactivity index. The HOMO-LUMO energy gap of 3.25, 3.26, 2.74 eV for (3a-c), reflects the chemical reactivity of these molecules.

A combined experimental and theoretical UV-Visible spectrum analysis of (3a) indicates that the first observed electronic transitions at  $\lambda = 244$  nm correspond to the electronic excitations calculated at  $\lambda = 295.39$  nm,  $f = 0.1662$ . The second observed  $\lambda_{\max}$  at 412 nm is in good agreement with the calculated  $\lambda_{\max} = 426.38$  nm,  $f = 0.9548$ . For (3b), the observed  $\lambda$  at 233, 389 nm agrees with the calculated electronic excitations at  $\lambda = 252.27$  nm,  $f = 0.4711$ ,  $\lambda = 416.01$  nm,  $f = 0.9518$ , respectively. The UV-Visible spectrum analysis of (3c) indicates that the observed  $\lambda$  at 242, 402 nm matches well with the electronic excitations calculated at  $\lambda = 252.47$  nm,  $f = 0.5936$ ;  $\lambda = 413.00$  nm,  $f = 0.8984$ , respectively. Therefore, the observed  $\lambda$  is slightly blue shifted compared with the calculated  $\lambda$ . On the basis of molecular orbital coefficients and molecular orbital plots the nature of electronic excitations for (3a) is assigned as  $\pi \rightarrow \pi^*$ , whereas for (3b), (3c) as  $n \rightarrow \pi^*$ .

A useful aspect of the NBOs is that it provides an accurate method for studying intramolecular bonding and interaction among bonds and also gives an efficient basis for investigating charge transfer or conjugative interaction in various molecular systems. Second-order perturbation theory analysis of the Fock matrix in NBO basis for (3a-c) is presented in Supplementary material (S Table 2a-c). In (3a-c), the interactions  $\pi(C2-C3) \rightarrow \pi^*(C4-C5)$ ,  $\pi(C4-C5) \rightarrow \pi^*(C2-C3)$  are responsible for the conjugation of respective  $\pi$ -bonds in pyrrole ring due to the high electron density at conjugated  $\pi$  bonds (1.666-1.678) and low electron density at  $\pi^*$  bonds (0.420-0.433) and stabilized the molecules with energy 83.01-95.60 kJ/mol. The interaction  $n_1(N1) \rightarrow \pi^*(C2-C3)/\pi^*(C4-C5)$  shows that lone pair of pyrrole N atom takes part in electron delocalization within ring. In the same manner, the  $\pi \rightarrow \pi^*$  interactions of benzene or pyridine ring designate the conjugation of respective  $\pi$ -bonds within ring and stabilized the molecules in a broad region 57.43-110.52 kJ/mol, due to presence of the different substituent at benzene ring as 2-OH, 3,5-NO<sub>2</sub>, for (3a), (3c) and pyridine ring in (3b), respectively. The interactions  $\pi(C2-C3) \rightarrow \pi^*(C6-C7)$ ,  $\pi(C6-C7) \rightarrow \pi^*(C2-C3)$  are responsible for the conjugation of bonds C2-C3, C6-C7 with C2-C6 and stabilized the molecule with energy

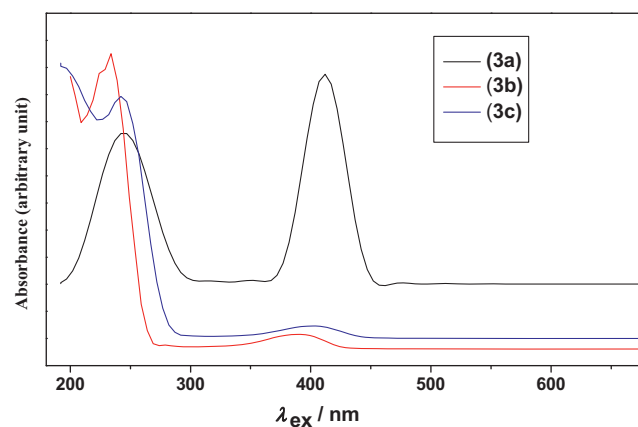


**Figure 2** The experimental UV-Visible spectra of (3a-c).

50.70–104.20 kJ/mol. In the same manner, the interactions  $\pi(\text{C4—C5}) \rightarrow \pi^*(\text{C15—N16})$  and  $\pi(\text{C15—N16}) \rightarrow \pi^*(\text{C4—C5})$  are responsible for the conjugation of these bonds with C5—C15. It is to be noticed that the charge transfer interactions are formed by the orbital overlap between bonding ( $\pi$ ) and antibonding ( $\pi^*$ ) orbitals, which results in intramolecular charge transfer (ICT) causing stabilization of the system. The movement of  $\pi$ -electron cloud from donor to acceptor *i.e.* intramolecular charge transfer (ICT) can make the molecules more polarized, which must be responsible for the NLO properties of molecules. Therefore, the titled compounds may be used for non-linear optical materials. The primary hyperconjugative interaction  $\pi_1(\text{C8—N9}) \rightarrow \sigma^*(\text{N1—H27})/\sigma^*(\text{N1—H26})/\sigma^*(\text{N1—H20})$  designates the intramolecular hydrogen bonding as N1—H27...N9, N1—H26...N9, N1—H20...N9 in molecules (3a–c), respectively. In (3a), the interaction  $n_2(\text{O19}) \rightarrow \sigma^*(\text{O26—H42})$  shows existence of intramolecular hydrogen bonding as O26—H42...O19. The presence of nitro group in (3c) stabilized the molecule to a greater extent of 679.30, 693.10 kJ/mol due to the interactions  $n_3(\text{O41}) \rightarrow \pi^*(\text{N40—O42})$ ,  $n_3(\text{O38}) \rightarrow \pi^*(\text{N37—O39})$ , respectively. In (3a–c), the secondary hyperconjugative interactions  $\sigma \rightarrow \sigma^*$  associated with pyrrole and benzene ring stabilized the molecules with energy 9.57–19.48 kJ/mol. Selected Lewis orbitals (occupied bond or lone pair) of (3a–c) with their NBO hybrid orbitals are listed in Supplementary material (S Table 3a–c). The NBO hybrid orbitals analysis shows that all the N—H/C—N bond orbitals are polarized toward the nitrogen atom (ED = 57.39 – 74.75% at N), whereas C—O/N—O bond orbitals toward oxygen atom (ED = 51.34 – 79.02% at O). The electron density distribution (occupancy) around the imino group ( $\text{>N—H}$ ) also influences the polarity of the compound. Therefore, they consist with the maximum electron density on the oxygen and nitrogen atoms, which is responsible for the polarity of the molecule.

#### 4.4. Emission (photoluminescence) spectroscopy

The optical properties of (3a–c) have been explored using electronic absorption and photoluminescence spectra. Quantum mechanically, Photoluminescence (PL) can be described as an excitation to a higher energy state and then a return to a lower energy state accompanied by the emission of a photon. The emitted radiation is generally of a longer wavelength than the wavelengths imposed on the photoluminescent material and difference between wavelength absorption maxima and wavelength emission maxima is known as the Stoke's shift.

For any photoluminescent species, the quantum yield ( $\Phi_F$ ) of its luminescence is a basic property, and its measurement is an important step in the characterization of the species. According to the definition of the  $\Phi_F$  (Brouwer, 2011), only two quantities need to be known, viz. the number of photons absorbed and the number of photons emitted per unit of time. The quantum yields ( $\Phi_F$ ) of (3a–c) were determined in dilute solutions with an absorbance below 0.1 at the excitation wavelength. Quinine sulfate (in 0.1 M  $\text{H}_2\text{SO}_4$   $\lambda_{ex} = 347$  nm,  $\Phi = 0.57$ ) was used as a standard (Lakowicz, 2006). Quantum yields were calculated using the following equation:

$$(\Phi_F) = [F^s \times f_r(\eta_s)^2 / F^r \times f_s(\eta_r)^2] \times \Phi_F^r$$

where  $F^s$  and  $F^r$  denote the area under the fluorescence band of sample and reference,  $f_r$  and  $f_s$  denote the absorbance at the

excitation wavelength of sample and reference, and  $\eta$  denotes the refractive index. Refractive index was calculated by the Lorentz–Lorentz equation ( $(4\pi/3) * (\alpha_i/V_{mol})$ ). Integration of the emission bands was performed using Origin 7.1.

The experimental emission spectra of (3a–c) were recorded in DMSO, at excitation  $\lambda_{ex,max}$ , and are shown in Fig. 3. The experimental PL spectral data of (3a–c) are listed in Table 2 with quantum yield. The most striking feature is that the (3a) gives an intense emission at  $\lambda_{em,max} = 572$  nm in yellow region upon irradiation by ultraviolet light  $\lambda_{ex,max} = 244$  nm, whereas another intense emission at  $\lambda_{em,max} = 521$  nm in green region upon irradiation by visible light  $\lambda_{ex,max} = 412$  nm. The compound (3b) gives two intense emissions at  $\lambda_{em,max} = 480, 522$  nm in blue and green region, respectively, upon irradiation by ultraviolet light  $\lambda_{ex,max} = 233$  nm. Another ultraviolet irradiation at  $\lambda_{ex,max} = 389$  nm gives also an intense emission at same  $\lambda_{em,max} = 480$  nm in blue region. The compound (3c) gives an intense emission at same  $\lambda_{em,max} = 520$  nm in green region upon irradiation by  $\lambda_{ex,max} = 242, 440$  nm. Therefore, the emission spectra show that (3a–c) are good photoluminescent material due to intense emission at higher wavelength in yellow, green and blue region with high Stoke's shift in the region 80–328 nm.

The data with the model compounds have shown that the quantum yield of aromatic hydrazone of 3a is essentially affected by an *ortho*-hydroxyl substituent. Furthermore, the compound 3c shows only one excitation peak at 402 and 442 excitation wavelengths.

#### 4.5. Vibrational band assignments

The aim of the vibrational analysis is to decide which of the vibrational modes in the molecule give rise to each of the observed bands at specific wave numbers in the FTIR spectra. The functional groups present in the molecule were identified and a satisfactory vibrational band assignment has been made for the fundamental modes of vibration by observing the position, shape and intensity of the bands. Vibrational frequencies of similar pyrrole hydrazones (Singh et al., 2013a, 2013b, 2013c, 2013d, 2013e, 2014a, 2014b; Rawat and Singh, 2015a, 2015b), compounds and their derivatives have been taken into consideration for the assignment of fundamental vibrations of

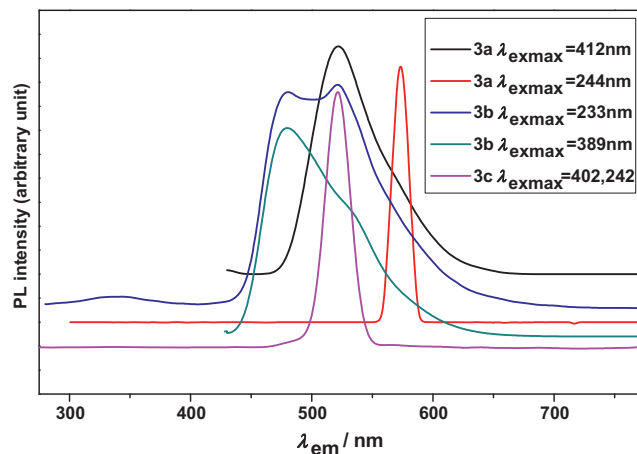


Figure 3 The experimental emission spectra of (3a–c).

**Table 2** Experimental PL spectral data of (3a–c) in DMSO:  $\lambda_{ex,max}$ : Excitation maxima wavelength,  $\lambda_{em,max}$ : emission maxima wavelength and S–Stoke's shifts, quantum yields ( $\Phi_F$ ).

	$\lambda_{ex,max}$ (nm)	$\lambda_{em,max}$ (nm)	S (nm)	( $\Phi_F$ )
(3a)	244	572(s) [yellow]	328	0.563
	412	521(s) [green]	109	0.269
(3b)	233	480(s) [blue]	247	0.411
		522(s) [green]	289	
	389	480(s) [blue]	91	0.432
(3c)	242, 402	520(s) [green]	278, 80	0.613

s–strong, m–medium, w–weak,  $S = [\lambda_{em,max} - \lambda_{ex,max}]$ .

studied compounds (3a–c). The theoretical (selected) and experimental vibrational modes of (3a–c), calculated at B3LYP/6-31G(d,p) method and their approximate assignments are given in Table 3. Comparison between experimental and theoretical IR spectra in the region 4000–400  $\text{cm}^{-1}$  is shown in Supplementary Fig. 7a–c. The calculated vibrational wave numbers are higher than their experimental values for the majority of the normal modes. Two factors may be responsible for the discrepancies between the experimental and computed wave numbers. The first is caused by the environment (gas and solid phase) and the second is due to the fact that the experimental values are an anharmonic wave numbers while the calculated values are harmonic ones. Therefore, calculated wave numbers are scaled down using scaling factor 0.9608 (Rawat and Singh, 2014a, 2014b, and 2019), to discard the anharmonicity present in real system.

#### 4.5.1. N–H and O–H vibrations

The N–H stretching of C=N–H group occurs in the region 3400–3100  $\text{cm}^{-1}$ . Usually the frequency of this vibration is decreased in the presence of hydrogen bond (Bellamy, 1975). In the FT-IR spectra of (3a–c), the N–H stretches of pyrrole ( $\nu_{\text{N1-H27/H26/H20}}$ ) are observed at 3463, 3422, 3460  $\text{cm}^{-1}$ , whereas these are calculated at 3448, 3451, 3450  $\text{cm}^{-1}$ , respectively. The observed pyrrole  $\nu_{\text{N-H}}$  deviates slightly from the free  $\nu_{\text{N-H}}$  of pyrrole at 3475  $\text{cm}^{-1}$ , reported in the literature (Giuliano et al., 2010). Therefore, the maximum red shift of 53  $\text{cm}^{-1}$  in observed  $\nu_{\text{N1-H27/H26/H20}}$  compared to the reported free  $\nu_{\text{N-H}}$  indicates the involvement of the pyrrole  $\nu_{\text{N-H}}$  group in hydrogen bonding. The theoretical IR spectra show that N–H wagging modes of pyrrole ( $\omega_{\text{N1-H27/26/20}}$ ) are moderately active at 626–8  $\text{cm}^{-1}$ , whereas these are observed at 668, 648, 663  $\text{cm}^{-1}$ , respectively. The N–H stretch of  $-\text{CH}=\text{N}-\underline{\text{NH}}-$  part ( $\nu_{\text{N17-H37/36/30}}$ ) is observed at 3237–3293  $\text{cm}^{-1}$ , whereas these are calculated at 3375–3397  $\text{cm}^{-1}$  in theoretical IR spectra. The N–H rocking and wagging modes of  $-\text{CH}=\text{N}-\underline{\text{NH}}-$  assigned at 1497–1504, 506–529  $\text{cm}^{-1}$  agree well with the observed band at 1470–1493, 461–497  $\text{cm}^{-1}$ , experimentally.

The non-hydrogen bonded or free hydroxyl group of phenols absorbs strongly in the 3700–3584  $\text{cm}^{-1}$  region. In *o*-hydroxy aryl acids and esters, the vibrational wave number of hydrogen-bonded O–H group shifts toward lower wave number up to 300  $\text{cm}^{-1}$  due to the presence of intramolecular hydrogen bonding (Silverstein and Webster, 1963). In (3a), the observed O–H stretching vibration ( $\nu_{\text{OH}}$ ) at 3286  $\text{cm}^{-1}$  agrees well with the hydrogen-bonded O–H group. Therefore, solid

state spectrum of (3a) attributes to the vibration of hydrogen-bonded O–H group.

#### 4.5.2. C–H vibrations

According to the Internal coordinate system recommended by Pulay et al. (1979),  $\text{CH}_2$  group associates with six types of vibrational frequencies. The scissoring and rocking deformations belong to polarized in-plane vibration, whereas wagging and twisting deformations belong to depolarized out-of-plane vibration. In (3a–c), a weak band for  $\nu_{as}\text{CH}_2$  calculated at 2983–2987  $\text{cm}^{-1}$  corresponds to the observed wave number at 2955–2960  $\text{cm}^{-1}$ . The observed band at 2955–2960  $\text{cm}^{-1}$  also matches with the reported band in the literature in the region 3000  $\pm$  50 (Gambino et al., 2007). The calculated  $\nu_s\text{CH}_2$  at 2945–6  $\text{cm}^{-1}$  matches well with the reported band in the literature in the region 2965  $\pm$  30, for symmetric C–H stretching vibrations of  $\text{CH}_2$  (Gambino et al., 2007). The ( $\delta_{sc}$ ) and ( $\omega$ ) deformation modes for ester  $\text{CH}_2$  assigned at 1471–1490, 1350  $\text{cm}^{-1}$  match well with the reported bands in the literature in the region 1455  $\pm$  55, 1350  $\pm$  85, respectively (Gambino et al., 2007). The calculated  $\nu_{as}\text{CH}_3$  and  $\nu_s\text{CH}_3$  at 3010–3017, 2936–2930  $\text{cm}^{-1}$  correspond to the reported band in the literature in the region 2985  $\pm$  25, 2970  $\pm$  30 for asymmetric, symmetric C–H stretching vibrations of  $\text{CH}_3$ , respectively. The calculated ester  $\nu_{as}\text{CH}_3$  at 3010–3017  $\text{cm}^{-1}$  also corresponds to the observed wave number at 2982–3024  $\text{cm}^{-1}$ , experimentally. In theoretical IR spectra, the wave numbers at 1440–2, 1382–3  $\text{cm}^{-1}$  display the  $\delta_{as}$  and  $\delta_s$  deformation modes of ester methyl, respectively. The calculated weak bands for  $\nu_{\text{C-H}}$  of benzene at 3066–3071  $\text{cm}^{-1}$  match well with the observed wave numbers at 3069–3071  $\text{cm}^{-1}$ . The Schiff base  $\nu_{\text{C-H}}$  stretches are assigned at 2943–7  $\text{cm}^{-1}$ , whereas these are observed at 2838–2869  $\text{cm}^{-1}$  in FT-IR spectrum. The observed Schiff base  $\nu_{\text{C-H}}$  stretches are responsible for the formation of hydrazone linkage in (3a–c).

#### 4.5.3. C $\equiv$ N vibrations

In theoretical IR spectra of (3a–c), the calculated wave numbers at 2226–2229  $\text{cm}^{-1}$  designate the presence of C $\equiv$ N stretching vibrations and match well with the observed wave numbers at 2216–2225  $\text{cm}^{-1}$ . The free C $\equiv$ N stretching vibrations are reported in the literature in the region 2240–2260  $\text{cm}^{-1}$  (Silverstein and Webster, 1963). Therefore, the red shift in the observed C $\equiv$ N stretches compared with the free C $\equiv$ N stretches indicates involvement of the C $\equiv$ N group in intramolecular hydrogen bonding.

#### 4.5.4. C=O and C–O vibrations

The ester carbonyl stretching vibration  $\nu_{\text{C=O}}$  is expected in the region 1750–1715  $\text{cm}^{-1}$  (Silverstein and Webster, 1963) and in the present study these modes are assigned at 1722–1729  $\text{cm}^{-1}$  using DFT calculation. The experimental FT-IR spectra of (3a–c) give this mode at 1694–1709  $\text{cm}^{-1}$ . The “C–O stretching vibrations” of esters actually consist of two asymmetrical coupled vibrations as  $\text{O}-\text{C}(=\text{O})-\text{C}$ ,  $\text{O}-\text{C}-\text{C}$  and these bands occur in the region 1300–1000  $\text{cm}^{-1}$  (Silverstein and Webster, 1963). The calculated wave number at 1083–4  $\text{cm}^{-1}$  demonstrates the  $\text{O}-\text{C}-\text{C}$  stretching vibration ( $\nu_{\text{O12-C13}}$ ) and corresponds to the observed wave numbers at 1057–

**Table 3** Theoretical (selected) and experimental vibrational wave numbers of (**3a–c**) calculated at B3LYP/6-31G(d,p) level and their approximate assignments.

<b>(3a)</b>		<b>(3b)</b>		<b>(3c)</b>		Approximate assignment
$\bar{\nu}$ calcd.	$\bar{\nu}$ exp.	$\bar{\nu}$ calcd.	$\bar{\nu}$ exp.	$\bar{\nu}$ calcd.	$\bar{\nu}$ exp.	
3448	3463	3451	3422	3450	3460	$\nu_{\text{N-H}}$ -pyrrole
3397	3286	3375	3237	3376	3293	$\nu_{\text{N-H}}$ -ArCONH
3164	3286	–	–	–	–	$\nu_{\text{O-H}}$ -hydroxyl
3140	3131	3129	–	3141	3069	$\nu_{\text{C-H}}$ -pyrrole
3066	3071	3071	3070	3070	3069	$\nu_{\text{C-H}}$ -benzene
3017	3024	3010	2989	3011	2982	$\nu_{\text{as}}$ -CH ester Me
2983	2960	2987	2957	2987	2955	$\nu_{\text{as}}$ -CH ester CH <sub>2</sub>
2943	2851	2947	2838	2947	2869	$\nu_{\text{C-H}}$ -Schiff base
2945	–	2946	–	2946	–	$\nu_{\text{s}}$ -CH ester CH <sub>2</sub>
2936	–	2940	–	2939	–	$\nu_{\text{s}}$ -CH ester Me
2226	2216	2229	2217	2228	2225	$\nu_{\text{C8N9}}$ -cyanide
1722	1709	1724	1707	1729	1694	$\nu_{\text{C10=O11}}$ -ester carbonyl
1667	1645	1730	1670	1725	1655	$\nu_{\text{C18=O19}}$ -ArCONH
1608	1591	1610	1588	1623	1640	$\nu_{\text{C15=N16}}$ -Schiff base
–	–	–	–	1598	1585	$\nu_{\text{as}}$ -NO <sub>2</sub>
1598	–	1582	–	1598	–	$\nu_{\text{C=C}}$ -benzene
1575	–	1577	1554	1578	1553	$\nu_{\text{C6=C7}}$ -vinyl
1534	1555	1533	–	1534	1530	$\nu_{\text{C=C}}$ -pyrrole
1504	1493	1497	1480	1500	1470	$\rho_{\text{NH}}$ -ArCONH
1475	–	1471	–	1490	–	$\delta_{\text{sc}}$ -ester CH <sub>2</sub>
1470	1424	1464	1424	1464	1423	$\nu_{\text{[CC+CN]}}$ -pyrrole ring
1442	–	1441	–	1440	–	$\delta_{\text{as}}$ -ester Me
1406	1408	1406	1407	1405	1405	$\nu_{\text{[CC+CN]}}$ -pyrrole ring
1382	–	1383	–	1383	–	$\delta_{\text{as}}$ -ester Me
1350	–	1350	–	1350	–	$\omega$ -ester CH <sub>2</sub>
–	–	–	–	1341	1343	$\nu_{\text{s}}$ -NO <sub>2</sub>
1326	1326	1319	1329	1303	1321	$\nu_{\text{[CC+CN]}}$ -pyrrole ring
1289	1294	1289	1287	1287	1286	$\delta_{\text{CCH}}$ -pyrrole
1242	1236	1235	1235	1241	1238	$\nu_{\text{C10O12}}$ -ester + $\delta_{\text{OCO}}$ -ester
1229	1191	1213	1196	1207	1199	$\nu_{\text{C18-N17}}$ -HN-COAr
1167	1145	1167	1148	1184	1139	[ $\delta_{\text{CCH}}$ + $\delta_{\text{CNH}}$ ]-pyrrole
1131	1095	1134	1093	1137	1098	$\nu_{\text{N16-N17}}$ -CH=N-NH-
1083	1057	1084	1064	1083	1059	$\nu_{\text{O12-C13}}$ -ester O-C-C
1035	1020	1036	1015	1037	1012	[ $\delta_{\text{CCH}}$ + $\delta_{\text{CNH}}$ ]-pyrrole
1008	–	1008	–	1008	–	$\nu_{\text{C13-C14}}$ + $\nu_{\text{O12-C13}}$
992	942	973	944	978	961	$\delta_{\text{trigonal}}$ -R1
905	905	907	876	933	938	$\omega_{\text{C15H38}}$ -Schiff base
884	884	887	842	897	875	[ $\delta_{\text{O19C18N17}}$ + $\delta_{\text{N16N17C18}}$ ]
869	–	870	–	869	–	$\omega_{\text{C-H}}$ -pyrrole
–	–	–	–	828	828	$\delta_{\text{NO2}}$ + $\omega_{\text{C-H}}$ -benzene
826	793	826	791	827	793	$\omega_{\text{C-H}}$ -benzene + $\delta_{\text{NO2}}$
767	745	768	756	769	759	$\delta$ -pyrrole ring + $\delta_{\text{C5C15N16}}$ + $\delta_{\text{C15N16N17}}$
725	696	724	720	740	738	$\delta_{\text{as}}$ -R1 + $\delta_{\text{oop}}$ -NO <sub>2</sub>
655	–	655	–	647	–	R1-puckering
626	668	628	648	628	663	$\omega_{\text{N-H}}$ -pyrrole
514	461	506	493	529	497	$\omega_{\text{N-H}}$ -ArCONH

Proposed assignment for different vibrational modes: Types of vibrations:  $\nu_{\text{s}}$  – symmetric stretching,  $\nu_{\text{as}}$  – asymmetric stretching,  $\delta_{\text{sc}}$  – scissoring,  $\rho$  – rocking,  $\omega$  – wagging,  $\delta$  – deformation,  $\delta_{\text{as}}$  – asymmetric deformation, R1 – benzene/pyridine ring.

1064  $\text{cm}^{-1}$ , experimentally. In theoretical IR spectra, a combination band of the 'O=C(=O)-C stretching vibration ( $\nu_{\text{C10-O12}}$ )' and 'ester O-C-O deformation' at 1235–1242  $\text{cm}^{-1}$  is in good agreement with the observed bands at 1235–8  $\text{cm}^{-1}$  in experimental FT-IR spectra. In (**3a**), (**3b**), (**3c**), ArCONH carbonyl stretches ( $\nu_{\text{C18=O19}}$ ) are observed at 1645, 1670, 1655  $\text{cm}^{-1}$ , respectively. Therefore, in (**3a**) the red shift in the observed  $\nu_{\text{C18=O19}}$  stretches compared with

the (**3b**), (**3c**) indicates involvement of the C18=O19 group of (**3a**) in hydrogen bonding.

#### 4.5.5. C=C, C-C vibrations

The calculated C=C stretches of benzene at 1582–1598  $\text{cm}^{-1}$  match well with the reported band in the literature in the region 1600–1585  $\text{cm}^{-1}$  (Gambino et al., 2007). The C=C stretches of pyrrole are assigned at 1533–4, 1464–1470  $\text{cm}^{-1}$ ,

whereas these DFT modes are observed at 1530–1555, 1423–4 cm<sup>-1</sup>, respectively. In DFT calculation, bands at 973–992 cm<sup>-1</sup> display the trigonal deformation of benzene ring ( $\delta$ -R1), whereas these are observed at 942–961 cm<sup>-1</sup>. The calculated modes at 1035–1037 cm<sup>-1</sup> designate to the  $\delta$ <sub>C–C–H</sub> associated with pyrrole and correspond to the observed wave numbers at 1012–1020 cm<sup>-1</sup>. The observed bands at 1553–4 cm<sup>-1</sup> designate the presence of the vinyl group ( $\nu$ <sub>C6=C7</sub>). The DFT mode at 1008 cm<sup>-1</sup> assigns to the C–C stretching vibration of ester ( $\nu$ <sub>C13–C14</sub>). In theoretical IR spectrum of (3a–c), a weak band for ring puckering vibration (a torsional mode) of benzene is assigned at 647–655 cm<sup>-1</sup>. The DFT modes for asymmetric deformation of benzene ( $\delta$ <sub>as</sub>-R1) at 724–740 cm<sup>-1</sup> agree well with the observed bands at 696–738 cm<sup>-1</sup>, experimentally.

#### 4.5.6. C=N, C–N and N–N vibrations

For (3a–c), Schiff base  $\nu$ <sub>C=N</sub> modes assigned at 1608–1623 cm<sup>-1</sup> correspond to the observed wave numbers at 1588–1640 cm<sup>-1</sup>, experimentally. The presence of the  $\nu$ <sub>C=N</sub> bands in (3a–c) confirms hydrazone linkage in all the investigated molecules. The calculated bands for  $\nu$ <sub>C=N</sub> also match with the reported band at 1602 cm<sup>-1</sup> in the literature (Gambino et al., 2007). The observed C–N stretches as  $\nu$ <sub>C18–N17</sub> at 1191–1199 cm<sup>-1</sup> are in agreement with the calculated wave numbers at 1207–1229 cm<sup>-1</sup>. The C–N stretching vibration is also active in the region 1275 ± 55 cm<sup>-1</sup>. The DFT modes for N–N stretches as  $\nu$ <sub>N16–N17</sub> at 1131–1137 cm<sup>-1</sup> correspond to the observed wave numbers at 1093–1098 cm<sup>-1</sup>.

#### 4.5.7. N=O vibrations

The molecules under investigation (3c) possess two nitro groups. The nitro groups show two types of stretching vibrations as asymmetric ( $\nu$ <sub>as</sub>) and symmetric ( $\nu$ <sub>s</sub>). The  $\nu$ <sub>as</sub> stretches are always observed at higher wave number than  $\nu$ <sub>s</sub> stretches. In (3c), the  $\nu$ <sub>as</sub> and  $\nu$ <sub>s</sub> stretches of nitro groups calculated at 1598, 1341 cm<sup>-1</sup> are in agreement with the observed wave numbers at 1585, 1343 cm<sup>-1</sup>, respectively. The  $\nu$ <sub>as</sub> and  $\nu$ <sub>s</sub> stretching vibrations of nitro group are also reported in the literature at 1600, 1319 cm<sup>-1</sup>, respectively (Silverstein and Webster, 1963). The calculated deformation modes of nitro groups at 827 cm<sup>-1</sup> are observed at the same wave number in experimental FT-IR spectrum.

#### 4.6. Quantum theory of atoms in molecules (QTAIM) analysis

Topological as well as geometrical parameters are useful tool to characterize the strength and nature of hydrogen bond (Bader, 1990; Lee et al., 1994). Molecular graphs of (3a–c) using AIM program at B3LYP functional are shown in Supplementary Fig. S8. Topological as well as geometrical parameters calculated at B3LYP/6-31G(g,p) and  $\omega$ B97X/6-31G(d,p) level for bonds of interacting atoms for 3a, 3b and 3c are given in Tables 4 and 5, respectively. For the intramolecular interactions N1–H27/H26/H20...N9 electron density ( $\rho_{H...A}$ ) and its Laplacian ( $\nabla^2\rho_{BCP}$ ) follow the Koch and Popelier (1995) criteria and the distance between interacting atoms ( $d_{H27/H26/H20...N9} = 2.44$ – $2.45$  Å) is less than the sum of van der Waals radii of these atoms. Therefore, these interactions are in the category of hydrogen bonds. The nature

of N1–H27/H26/H20...N9 hydrogen bonds is weak due to ( $\nabla^2\rho_{BCP}$ ) > 0 and  $H_{BCP} > 0$ , whereas O26–H42...O19 is a medium hydrogen bond due to ( $\nabla^2\rho_{BCP}$ ) > 0 and  $H_{BCP} < 0$ . In this article, QTAIM theory is used to estimate hydrogen bond energy ( $E$ ), and the energy of intramolecular hydrogen bonds N1–H27/H26/H20...N9, O26–H42...O19 is calculated as 9.23, 9.23, 9.41, 55.72 kJ/mol, respectively. In (3a), the presence of bond critical point (BCP) at H37...H38 contact designates presence of the dihydrogen bonding due to short  $d_{H37...H38}$  of 1.97 Å. Energy of hydrogen bonding is calculated using AIM and DFT calculations. With respect to change of both the method used and the basis set the reliability and stability of values of QTAIM parameters have been studied and found that they were almost independent of basis set in case of used B3LYP functional in DFT (Jablonski and Palusiak, 2010). Energy of hydrogen bonding has been calculated using both B3LYP functional and  $\omega$ B97X with 6-31G(d,p) basis set for describing hydrogen bond interactions in molecules. The calculated values tabulated in Tables 4 and 5 found to vary only slightly.

#### 4.7. Chemical reactivity

The chemical reactivity of molecule is described in three ways as: (i) Molar refractivity (MR) and (ii) Global and local electronic reactivity descriptors.

##### 4.7.1. Molar refractivity (MR)

Molar refractivity (MR) is an important property used in quantitative structure property relationship (QSPR). It is directly related to the refractive index, molecular weight and density of steric bulk and responsible for the lipophilicity and binding property of investigated system. It can be calculated by the Lorentz–Lorentz equation (Padrón et al., 2002; Verma and Hansch, 2005) and defined as

$$MR = [(n^2 - 1)(n^2 + 2)].(MW/\rho) = 1.333\pi N\alpha_0$$

where  $n$  is the refractive index,  $MW$  is the molecular weight,  $\rho$  is the density,  $(MW/\rho)$  is the molar volume,  $N$  is the Avogadro Number, and  $\alpha_0$  is the polarizability of molecular system. This equation holds for both liquid state and solid state of system. Using this equation, the molar refractivity (MR) for (3a–c) has been calculated as 109.28, 102.96, 119.14 esu, respectively. Molar refractivity is found to be related to the London dispersive forces that act in the drug–receptor interaction (Padrón et al., 2002). The molar refractivity has been reported as an important parameter in modulating the antimalarial activity (Uniyal et al., 2010), through charge transfer between drug and globin protein, indicating that the studied compounds may have activity against malarial disease. Molar refractivity based binding property of 4-Quinolinylnyl and 9-Acrydinylnyl hydrazones has been found to be potent antimalarial agents and active against C–Q resistant clone K1 Plasmodium falciparum strain (Uniyal et al., 2010).

##### 4.7.2. Electronic reactivity descriptors

4.7.2.1. Global and Local reactivity descriptors. The chemical reactivity and site selectivity of the molecular systems have been determined on the basis of Koopman's theorem (Parr and Yang, 1989). Global reactivity descriptors as electronegativity ( $\chi$ ) =  $-1/2(\epsilon_{LUMO} + \epsilon_{HOMO})$ , chemical potential

**Table 4** Topological parameters for intramolecular interactions at B3LYP functional and  $\omega$ B97X in (**3a–c**): electron density ( $\rho_{\text{BCP}}$ ), Laplacian of electron density ( $\nabla^2\rho_{\text{BCP}}$ ), electron kinetic energy density ( $G_{\text{BCP}}$ ), electron potential energy density ( $V_{\text{BCP}}$ ), total electron energy density ( $H_{\text{BCP}}$ ), Hydrogen bond energy ( $E_{\text{HB}}$ ) at bond critical point (BCP).

B3LYP/6-31G(d,p)							
	Interactions	$\rho_{\text{BCP}}$	$\nabla^2\rho_{\text{BCP}}$	$G_{\text{BCP}}$	$V_{\text{BCP}}$	$H_{\text{BCP}}$	$E_{\text{HB}}$
<b>(3a)</b>	O26—H42...O19	0.0515	0.1487	0.0398	−0.0424	−0.0026	−13.30
	N1—H27...N9	0.0118	0.0428	0.0088	−0.0070	0.00184	−2.196
	H37...H38	0.0128	0.0543	0.0109	−0.0082	0.00267	−2.572
<b>(3b)</b>	N1—H26...N9	0.0118	0.0428	0.0088	−0.0070	0.0018	−2.196
<b>(3c)</b>	N1—H20...N9	0.0120	0.0435	0.0090	−0.0071	0.0018	−2.227
$\omega$ B97X/6-31G(d,p)							
<b>(3a)</b>	O26—H42...O19	0.0475	0.1439	0.0375	−0.0390	−0.0015	−12.26
	N1—H27...N9	0.0121	0.0445	0.0092	−0.0074	0.0018	−2.329
	H37...H38	0.0126	0.0556	0.0110	−0.0081	0.00287	−2.564
<b>(3b)</b>	N1—H26...N9	0.01212	0.0443	0.0092	−0.0073	0.0018	−2.315
<b>(3c)</b>	N1—H20...N9	0.01213	0.0443	0.0092	−0.0074	0.0018	−2.323

$\rho_{\text{BCP}}$ ,  $\nabla^2\rho_{\text{BCP}}$ ,  $G_{\text{BCP}}$ ,  $V_{\text{BCP}}$ ,  $H_{\text{BCP}}$  in a.u. and  $E_{\text{HB}}$  in (kJ/mol).

**Table 5** Geometrical parameters for intramolecular interaction at B3LYP functional and  $\omega$ B97X in (**3a–c**): bond distance (Å), bond angle (°) and sum of van der Waal radii of interacting atoms (Å).

B3LYP/6-31G(d,p)						
	Interactions (D—H...A)	$d_{\text{D—H}}$ (Å)	$d_{\text{H...A}}$ (Å)	$d_{\text{D...A}}$ (Å)	D—H...A (°)	$(r_{\text{H}} + r_{\text{A}})$ (Å)
<b>(3a)</b>	N1—H27...N9	1.01	2.45	3.31	141.90	2.75
	O26—H42...O19	0.99	1.66	2.56	148.17	2.72
	H37...H38	—	1.97	—	—	—
<b>(3b)</b>	N1—H26...N9	1.01	2.45	3.31	141.89	2.75
<b>(3c)</b>	N1—H20...N9	1.01	2.44	3.30	142.12	2.75
$\omega$ B97X/6-31G(d,p)						
<b>(3a)</b>	N1—H27...N9	1.01	2.44	3.29	141.73	2.75
	O26—H42...O19	0.98	1.69	2.57	147.03	2.72
	H37...H38	—	2.00	—	—	—
<b>(3b)</b>	N1—H26...N9	1.01	2.44	3.29	141.58	2.75
<b>(3c)</b>	N1—H20...N9	1.01	2.45	3.31	142.02	2.75

( $\mu$ ) =  $1/2 (\epsilon_{\text{LUMO}} + \epsilon_{\text{HOMO}})$ , global hardness ( $\eta$ ) =  $1/2 (\epsilon_{\text{LUMO}} - \epsilon_{\text{HOMO}})$ , global softness ( $S$ ) =  $1/2\eta$  and electrophilicity index ( $\omega$ ) =  $\mu^2/2\eta$  are highly successful in predicting global reactivity trends (Rawat and Singh, 2014a, 2014b, 2019; Singh et al., 2013a, 2013b, 2013c, 2013d, 2013e; Singh and Rawat, 2013). According to Parr et al., electrophilicity index ( $\omega$ ) is a global reactivity index similar to the chemical hardness and chemical potential. This is positive and definite quantity and measures the stabilization in energy when the system acquires an additional electronic charge ( $\Delta N$ ) from the environment. The energies of frontier molecular orbitals ( $\epsilon_{\text{HOMO}}$ ,  $\epsilon_{\text{LUMO}}$ ), energy gap ( $\epsilon_{\text{LUMO}} - \epsilon_{\text{HOMO}}$ ), electronegativity ( $\chi$ ), chemical potential ( $\mu$ ), global hardness ( $\eta$ ), global softness ( $S$ ), global electrophilicity index ( $\omega$ ) for (**1**), (**2a–c**), (**3a–c**) and ECT for reactant systems as [**1**  $\leftrightarrow$  **2a**], [**1**  $\leftrightarrow$  **2b**], [**1**  $\leftrightarrow$  **2c**] are listed in Table 6. The global electrophilicity index ( $\omega = 5.41, 5.50, 8.11$  eV) for (**3a–c**) shows that they behave as strong electrophiles and their electrophilic power is in the following order as (**3a**) < (**3b**) < (**3c**).

Electrophilic charge transfer (ECT) =  $(\Delta N_{\text{max}})_A - (\Delta N_{\text{max}})_B$  is defined as the difference between the  $\Delta N_{\text{max}}$  values of interacting molecules A and B. If we consider two molecules A and B approach to each other (i) if ECT > 0, charge flow

from B to A (ii) if ECT < 0, charge flow from A to B. ECT is calculated as 1.04, 0.96, 0.03 for reactant systems [**1**  $\leftrightarrow$  **2a**], [**1**  $\leftrightarrow$  **2b**], [**1**  $\leftrightarrow$  **2c**], respectively *i.e.* ECT > 0, which indicates that charge flows from (**2a–c**) to (**1**). Therefore, (**1**) acts as global electrophile and (**2a–c**) as global nucleophile.

Selected electrophilic reactivity descriptors ( $f_k^+$ ,  $s_k^+$ ,  $\omega_k^+$ ) for reactant (**1**) and nucleophilic reactivity descriptors ( $f_k^-$ ,  $s_k^-$ ,  $\omega_k^-$ ) for reactants (**2a–c**), using Hirshfeld charges are given in Table 7. The maximum values of local electrophilic reactivity descriptors ( $f_k^+$ ,  $s_k^+$ ,  $\omega_k^+$ ) at aldehyde carbon C6 of reactant (**1**) indicate that this is the most electrophilic site. The nucleophilic reactivity descriptors ( $f_k^-$ ,  $s_k^-$ ,  $\omega_k^-$ ) of reactant (**2a–c**) show that N atom of  $\text{NH}_2$  (N10) is the most nucleophilic site. Therefore, the nucleophilic attack of N10 of reactant (**2a–c**) at the most electrophilic site C6 of reactant (**1**) confirms the formation of product molecules or Schiff base linkage (C15=N16) in aroylhydrazones (**3a–c**). Selected reactivity descriptors as Fukui functions ( $f_k^+$ ,  $f_k^-$ ), local softnesses ( $s_k^+$ ,  $s_k^-$ ), local electrophilicity indices ( $\omega_k^+$ ,  $\omega_k^-$ ) for (**3a–c**), using Mulliken atomic charges are given in Table 8. The maximum values of local electrophilic reactivity descriptors ( $f_k^+$ ,  $s_k^+$ ,  $\omega_k^+$ ) at vinyl carbon (C6) of (**3a–c**) indicate that this site is more prone to nucleophilic attack and favors

**Table 6** Calculated ( $\epsilon_{\text{HOMO}}$ ,  $\epsilon_{\text{LUMO}}$ ), energy band gap ( $\epsilon_{\text{LUMO}} - \epsilon_{\text{HOMO}}$ ), electronegativity ( $\chi$ ), chemical potential ( $\mu$ ), global hardness ( $\eta$ ), global softness ( $S$ ) and global electrophilicity index ( $\omega$ ) for **(1)**, **(2a-c)**, **(3a-c)** and Electrophilic charge transfer (ECT) for reactant systems [**1**  $\leftrightarrow$  **2a**], [**1**  $\leftrightarrow$  **2b**], [**1**  $\leftrightarrow$  **2c**].

	$\epsilon_{\text{H}}$	$\epsilon_{\text{L}}$	$\epsilon_{\text{L}} - \epsilon_{\text{H}}$	$\chi = -\mu$	$\eta$	$S$	$\omega$	ECT
<b>(1)</b>	-6.5133	-2.8547	3.6585	4.6840	1.8293	0.2733	5.9969	
<b>(2a)</b>	-6.1057	-1.2585	4.8472	3.6821	2.4236	0.2063	2.7971	(1.0412) <sub>[1<math>\leftrightarrow</math>2a]</sub>
<b>(3a)</b>	-5.8276	-2.5710	3.2561	4.1995	1.6283	0.3071	5.4163	
<b>(2b)</b>	-7.121	-1.633	5.487	4.377	2.743	0.182	3.492	(0.965) <sub>[1<math>\leftrightarrow</math>2b]</sub>
<b>(3b)</b>	-5.876	-2.606	3.269	4.241	1.634	0.305	5.501	
<b>(2c)</b>	-7.6391	-3.3064	4.3326	5.4727	2.1664	0.2308	6.9130	(0.0342) <sub>[1<math>\leftrightarrow</math>2c]</sub>
<b>(3c)</b>	-6.0934	-3.3483	2.7451	4.7209	1.3726	0.3642	8.1189	

$\epsilon_{\text{H}}$ ,  $\epsilon_{\text{L}}$ ,  $\epsilon_{\text{H}} - \epsilon_{\text{L}}$ ,  $\chi$ ,  $\mu$ ,  $\eta$ ,  $\omega$  (in eV) and  $S$  (in eV<sup>-1</sup>).

**Table 7** Selected electrophilic reactivity descriptors ( $f_k^+$ ,  $s_k^+$ ,  $\omega_k^+$ ) for reactant **(1)** and nucleophilic reactivity descriptors ( $f_k^-$ ,  $s_k^-$ ,  $\omega_k^-$ ) for reactants **(2a-c)**, using Hirshfeld charges.

	Sites	$f_k^+$	$s_k^+$	$\omega_k^+$		Sites	$f_k^-$	$s_k^-$	$\omega_k^-$
<b>(1)</b>	C6	0.1170	0.0320	0.7021	<b>(2a)</b>	N9	0.0459	0.0095	0.1281
	C12	0.0384	0.0105	0.2307		N10	0.0672	0.0140	0.1873
					<b>(2b)</b>	N9	0.1579	0.0287	0.5515
						N10	0.2914	0.0530	1.0176
					<b>(2c)</b>	N9	0.1066	0.0246	0.7374
						N10	0.1312	0.0302	0.9071

$f_k^+$ ,  $f_k^-$  (in e);  $s_k^+$ ,  $s_k^-$  (in eV<sup>-1</sup>) and  $\omega_k^+$ ,  $\omega_k^-$  (in eV).

**Table 8** Selected reactivity descriptors as Fukui functions ( $f_k^+$ ,  $f_k^-$ ), local softnesses ( $s_k^+$ ,  $s_k^-$ ), local electrophilicity indices ( $\omega_k^+$ ,  $\omega_k^-$ ) for products **(3a-c)**, using Mulliken atomic charges.

	Sites	$f_k^+$	$s_k^+$	$\omega_k^+$		Sites	$f_k^-$	$s_k^-$	$\omega_k^-$
<b>(3a)</b>	C6	0.0556	0.0170	0.3011	<b>(3a)</b>	N1	0.0005	0.0001	0.0031
	C10	0.0434	0.0133	0.2350		N17	0.0277	0.0085	0.1504
	C15	0.0411	0.0126	0.2230		<b>(3b)</b>	N1	0.0005	0.0002
C18	0.0354	0.0108	0.1921	N17	0.039		0.012	0.216	
<b>(3b)</b>	C6	0.052	0.016	0.289	<b>(3c)</b>	N1	0.00047	0.00017	0.00384
	C10	0.041	0.012	0.227		N17	0.03379	0.01231	0.27436
	C15	0.040	0.012	0.222					
<b>(3c)</b>	C18	0.037	0.011	0.203					
	C6	0.03070	0.01118	0.24926					
	C10	0.02457	0.00895	0.19951					
	C15	0.02466	0.00898	0.20021					
	C18	0.02351	0.00856	0.19091					

$f_k^+$ ,  $f_k^-$  (in e);  $s_k^+$ ,  $s_k^-$  (in eV<sup>-1</sup>) and  $\omega_k^+$ ,  $\omega_k^-$  (in eV).

formation of the new unsymmetrical dipyrromethanes by attack of 2-unsubstituted pyrrole nucleophile at (C6). In the same way, for **(3a-c)** the maximum values of the nucleophilic reactivity descriptors ( $f_k^-$ ,  $s_k^-$ ,  $\omega_k^-$ ) at N17 nitrogen atom of  $-\text{CH}=\text{N}-\underline{\text{NH}}-$  indicate that this site is more prone to electrophilic attack.

#### 4.8. Static dipole moment ( $\mu_0$ ), mean polarizability ( $|\alpha_0|$ ), anisotropy of polarizability ( $\Delta\alpha$ ) and first hyperpolarizability ( $\beta_0$ )

As hyperpolarizability is difficult task to measure directly, computational calculation is an alternate choice and provides

another method to investigate extensive properties of materials. Polarizabilities and hyperpolarizabilities are described as response of a system in the presence of an applied electric field (Kleinmann, 1962). In order to investigate the relationship between molecular structure and NLO response, first hyperpolarizability ( $\beta_0$ ) of this novel molecular system, and related properties ( $|\alpha_0|$  and  $\Delta\alpha$ ) are calculated using B3LYP/6-31G(d,p), based on the finite-field approach and their calculated values are given in Table 9. Total static dipole moment ( $\mu_0$ ), mean polarizability ( $|\alpha_0|$ ), anisotropy of polarizability ( $\Delta\alpha$ ) and first hyperpolarizability ( $\beta_0$ ), using  $x$ ,  $y$ ,  $z$ , components are defined as

**Table 9** Calculated Dipole moment ( $\mu_0$ ), Polarizability ( $|\alpha_0|$ ), anisotropy of Polarizability ( $\Delta\alpha$ ), First Hyperpolarizability ( $\beta_0$ ) and their components for (**3a–c**), using B3LYP/6-31G(d, p).

	(3a)	(3b)	(3c)		(3a)	(3b)	(3c)
$\mu_x$	-1.942	-0.733	-2.707	$\beta_{xxx}$	3117.61	578.17	2965.32
$\mu_y$	5.625	5.057	-5.255	$\beta_{xxy}$	-1200.40	-1768.19	2380.40
$\mu_z$	0.236	-0.329	-1.187	$\beta_{xyy}$	22.32	-170.65	402.86
$(\mu_0)$	5.955	5.120	6.030	$\beta_{yyy}$	230.2	138.96	-23.53
$\alpha_{xx}$	490.42	453.52	519.90	$\beta_{xxx}$	26.76	30.69	487.92
$\alpha_{yy}$	291.82	271.67	319.86	$\beta_{yyz}$	-8.39	-24.50	-37.79
$\alpha_{zz}$	94.68	100.93	116.25	$\beta_{xzz}$	11.81	18.18	7.99
$ \alpha_0 $	43.31	40.81	47.22	$\beta_{yzz}$	1.94	-8.92	-6.13
$(\Delta\alpha)$	135.74	124.90	143.15	$\beta_{zzz}$	8.75	6.02	9.06
				$(\beta_0)$	28.48	14.62	35.76

$$\mu_0 = (\mu_x^2 + \mu_y^2 + \mu_z^2)^{1/2}$$

$$|\alpha_0| = 1/3(\alpha_{xx} + \alpha_{yy} + \alpha_{zz})$$

$$\Delta\alpha = 2^{-1/2}[(\alpha_{xx} - \alpha_{yy})^2 + (\alpha_{yy} - \alpha_{zz})^2 + (\alpha_{zz} - \alpha_{xx})^2 + 6\alpha_{xx}^2]^{1/2}$$

$$\beta_0 = [(\beta_{xxx} + \beta_{xxy} + \beta_{xyy})^2 + (\beta_{yyz} + \beta_{xyy} + \beta_{yzz})^2 + (\beta_{zzz} + \beta_{xzz} + \beta_{yzz})^2]^{1/2}$$

Large value of particular component of the polarizability and hyperpolarizability indicates a substantial delocalization of charge in these directions. Since the value of the polarizability ( $|\alpha_0|$ ) and first hyperpolarizability ( $\beta_0$ ) of Gaussian 09 output is reported in atomic unit (a.u.) these values are converted into electrostatic unit (esu) using converting factors as for  $\alpha_0$ : 1 a.u. =  $0.1482 \times 10^{-24}$  esu; for  $\beta_0$ : 1 a.u. =  $0.008639 \times 10^{-30}$  esu. The first hyperpolarizabilities ( $\beta_0$ ) of the title molecules (**3a–c**) are calculated as 28.48, 14.62,  $35.76 \times 10^{-30}$  esu, respectively with respect to *p*-Nitroaniline (*p*-NA) as a reference. The first hyperpolarizabilities of (**3a–c**) have been found to increase with electron withdrawing substituents and might be used as non-linear optical (NLO) material.

## 5. Conclusions

In this study we have presented a combined spectroscopic and quantum chemical studies on newly synthesized (**3a–c**) aroyl hydrazones. The calculated  $^1\text{H}$  and  $^{13}\text{C}$  NMR chemical shifts are in agreement with the observed chemical shifts, experimentally. A combined experimental and theoretical UV–Visible spectral analysis indicates that observed wavelength absorption maxima ( $\lambda_{ex,max}$ ) have blue shifts compared to the calculated  $\lambda_{ex,max}$  values. The molecular orbital coefficients and molecular orbital plots analysis suggests that the nature of electronic excitations involved in (**3a**) as  $\pi \rightarrow \pi^*$ , whereas for (**3b**), (**3c**) as  $n \rightarrow \pi^*$ . The emission spectra of (**3a–c**) show that title compounds are good photoluminescent material due to intense emission in green region and (**3a**), (**3b**) also show intense emission in yellow, blue region, respectively. The  $^1\text{H}$  NMR, NBO as well as vibrational analysis of (**3a–c**) are responsible for hydrogen bonding  $\text{N1–H27/26/20} \cdots \text{N9}$  due to downfield chemical shift,  $\pi_1(\text{C8–C9}) \rightarrow \sigma^*(\text{N1–H27/H26/H20})$  interaction and vibrational red shift in the wave number of both proton donor pyrrole N–H and proton acceptor  $\text{C}\equiv\text{N}$ , respectively. AIM calculation also confirms the presence of these hydrogen bonds due to existence of the bond critical point at  $\text{H27/26/20} \cdots \text{N9}$  contact. Topological criteria ( $\nabla^2\rho_{\text{BCP}} > 0$  and  $H_{\text{BCP}} > 0$ ) show that nature of these

hydrogen bonds is weak. The global electrophilicity index ( $\omega = 5.41, 5.50, 8.11$  eV) for (**3a–c**) indicates that these molecules behave as strong electrophiles. The electrophilic reactivity descriptors ( $f_k^+$ ,  $s_k^+$ ,  $\omega_k^+$ ) of (**3a–c**) indicate that the investigated molecules might be used as precursor for the target synthesis of new unsymmetrical dipyrromethane derivatives. These compounds exhibit strong effective intramolecular charge transfer (ICT) due to movement of  $\pi$ -electron cloud from donor to acceptor *i.e.* shows high polarity and responsible for the NLO properties of molecules. The first hyperpolarizabilities for (**3a–c**) ( $\beta_0 = 28.48, 14.62, 35.76 \times 10^{-30}$  esu) show that title molecules can be used as attractive material for non-linear optical (NLO) applications.

## Acknowledgments

Authors are thankful to CSIR for financial support.

## Appendix A. Supplementary material

Supplementary data associated with this article can be found, in the online version, at <http://dx.doi.org/10.1016/j.arabj.2015.03.001>.

## References

- Ajani, O.O., Obafemi, C.A., Nwinyi, O.C., Akinpelu, D.A., 2010. Microwave assisted synthesis and antimicrobial activity of 2-quinoxalinone-3-hydrazone derivatives. *Bioorg. Med. Chem.* 18, 214–221.
- Armbruster, F., Klingebiel, U., Noltemeyer, M.Z., 2006. Von Ketazinen zu 1,2-Diaza-3-phospha-cyclopent-5-enen,-penta-3,5-dienen,1,5-Diaza-2,6-diphospha-bicyclo[3.3.0]octa-3,7-dienund einem Cyclohexaphosphan. *Naturforsch.* 61b, 225–236.
- Bader, R.F.W., 1990. *Atoms' in Molecules. A Quantum Theory*. Oxford University Press, Oxford.
- Bedia, K.K., Seda, V.O.E., Fatma, K., Nathaly, S., Sevim, R., Dimoglo, A., 2006. Synthesis and characterization of novel hydrazide-hydrazones and the study of their structure-antituberculosis activity. *Eur. J. Med. Chem.* 41, 1253–1261.
- Bellamy, L.J., 1975. *The Infrared Spectra of Complex Molecules*, third ed. Chapman and Hall, London.
- Blau, W., 1987. Organic materials for nonlinear optical devices. *Phys. Technol.* 18, 250–268.

- Brouwer, A.M., 2011. Standards for photoluminescence quantum yield measurements in solution. *Pure Appl. Chem.* 8, 2213–2228.
- Chalapathi, P.V., Prathima, B., Rao, Y.S., Reddy, K.J., Ramesh, G.N., Reddy, D.V.R., Reddy, A.V., 2011. *Res. J. Chem. Environ.* 15, 579–585.
- Darnell, G., Richardson, D.R., 1999. The potential of iron chelators of the pyridoxal isonicotinoyl hydrazone class as effective antiproliferative agents III: the effect of the ligands on molecular targets involved in proliferation. *Blood* 94, 781–792.
- Dimmock, J.R., Vashishtha, S.C., Stables, J.P., 2000. Anticonvulsant properties of various acetylhydrazones, oxamoylhydrazones and semicarbazones derived from aromatic and unsaturated carbonyl compounds. *Eur. J. Med. Chem.* 35, 241–248.
- Frisch, M.J., et al. Gaussian 09, Revision B.01, Gaussian Inc., Wallingford, CT, 2010.
- Gambino, D., Otero, L., Vieites, M., Boiani, M., Gonzalez, M., Baran, E.J., Cerecetto, H., 2007. Vibrational spectra of palladium 5-nitrofuryl thiosemicarbazone complexes: experimental and theoretical study. *Spectrochim. Acta Part A* 68, 341–348.
- Gauss-View 5.09 Program. Gaussian Inc., Wallingford, CT, 06492 USA.
- Genger, U.R., Pfeifer, D., Hoffmann, K., Flachenecker, G., Hoffman, A., Monte, C., 2008. In: Wolfbeis, O.S. (Ed.), *Springer Series on Fluorescence*, vol. 5. Springer, Berlin, pp. 65–99.
- Giuliano, B.M., Reva, I., Fausto, R., 2010. Infrared spectra and photochemistry of matrix-isolated pyrrole-2-carbaldehyde. *J. Phys. Chem. A* 114, 2506–2517.
- Gup, R. and Kirkan, B., 2005. Synthesis and spectroscopic studies of copper(II) and nickel(II) complexes containing hydrazone ligands and heterocyclic coligand. 62, 1188–1195.
- Gursoy, A., Terzioglu, N., Otuk, G., 1997. Synthesis of some new hydrazide-hydrazones, thiosemicarbazides and thiazolidinones as possible antimicrobials. *Eur. J. Med. Chem.* 32, 753–757.
- Harmjanz, M., Gill, H.S., Scott, M.J., 2000. Porphodimethenoporphyrin interconversion: a tetrapyrrolic redox-switchable macrocycle. *J. Am. Chem. Soc.* 122, 10476–10477.
- Hayes, R.T., Wasilewski, M.R., Gosztola, D., 2000. Ultrafast photoswitched charge transmission through the bridge molecule in a donor–bridge–acceptor system. *J. Am. Chem. Soc.* 122, 5563–5567.
- Jablonski, M., Palusiak, M., 2010. Basis set and method dependence in atoms in molecules calculations. *J. Phys. Chem. A* 114, 2240–2244.
- Kavlentis, E., 1988. Synthesis of phthalaldehyde bisguanyldiazone (PABGH). Spectrophotometric analysis of Co(II)–Cu(II)–Ni(II) mixtures in the presence of several cations. *Anal. Lett.*, 21, 689–697.
- Kim, D. Hee, Eun, H.M., Choi, Ho.-Soeb., 2000. Density functional theory/GIAO/CSGT studies of the 13 C NMR chemical shifts in 1-chlorosilatrane. *Bull. Korean Chem. Soc.* 21, 148–150.
- Kjell, O., Per-Åke, P., 1979. Synthesis of pyrroles and a 1,2-Dihydropyrrolo[1,2-a]pyrazin-3(4H)-one identified as maillard reaction products. *Acta Chem. Scand. B* 33, 125–132.
- Kleinmann, D.A., 1962. Nonlinear dielectric polarization in optical media. *Phys. Rev.* 126, 1977–1979.
- Koch, U., Popelier, P.L.A., 1995. Characterization of C–H–O Hydrogen Bonds on the Basis of the Charge Density. *J. Phys. Chem.* 99, 9747–9754.
- Lakowicz, Joseph R., 2006. *Principles of Fluorescence Spectroscopy*, third ed. Springer Science & Business Media, Singapore.
- Lee Jr., J.C., Peris, E., Rheingold, A.L., Crabtree, R.H., 1994. An unusual type of H–H interaction: Ir–H–H–O and Ir–H–H–N hydrogen bonding and its involvement in  $\sigma$ -bond metathesis. *J. Am. Chem. Soc.* 116, 11014–11019.
- Melnyk, P., Leroux, V., Serhergert, C.P., 2006. Design, synthesis and in vitro antimalarial activity of an acylhydrazone library. *Bioorg. Med. Chem. Lett.* 16, 31–35.
- Mohareb, R.M., Ibrahim, R.A., Moustafa, H.E., 2010. Hydrazide-hydrazones in the synthesis of 1,3,4-oxadiazine, 1,2,4-triazine and pyrazole derivatives with anti-tumor activities. *Open. Org. Chem. J.* 4, 8–14.
- Murukan, B., Mohanan, K., 2007. Synthesis, characterization and antibacterial properties of some trivalent metal complexes with [(2-hydroxy-1-naphthaldehyde)-3-isatin]-bishydrazone. *J. Enzyme Inhib. Med. Chem.* 22, 65–70.
- Padrón, J.A., Carasco, R., Pellón, R.F., 2002. Molecular descriptor based on a molar refractivity partition using Randic-type graph-theoretical invariant. *J. Pharm. Pharmaceut. Sci.* 5, 258–266.
- Parr, R.G., Yang, W., 1989. *Density Functional Theory of Atoms and Molecules*. Oxford University Press, Oxford, New York.
- Pulay, P., Fogarasi, G., Pang, F., Boggs, J.E., 1979. Systematic ab initio gradient calculation of molecular geometries, force constants, and dipole moment derivatives. *J. Am. Chem. Soc.* 101, 2550–2560.
- Rallas, S., Gulerman, N., Erdeniz, H., 2002. Synthesis and antimicrobial activity of some new hydrazones of 4-fluorobenzoic acid hydrazide and 3-acetyl-2,5-disubstituted-1,3,4-oxadiazolines. *IL FARMACO* 57, 171–174.
- Rawat, P., Singh, R.N., 2014b. Spectral analysis, structural elucidation and evaluation of chemical reactivity of synthesized ethyl-4-[(2-cyano-acetyl)-hydrazonomethyl]-3,5-dimethyl-1H-pyrrole-2-carboxylate through experimental studies and quantum chemical calculations. *J. Mol. Struct.* 1074, 201–212.
- Rawat, P., Singh, R.N., 2014c. Evaluation of molecular assembly, spectroscopic interpretation, intra-/inter molecular hydrogen bonding and chemical reactivity of two pyrrole precursors. *J. Mol. Struct.* 1075, 462–470.
- Rawat, P., Singh, R.N., 2015a. Assessment of conformational, spectral, antimicrobial activity, chemical reactivity and NLO application of Pyrrole-2, 5-dicarboxaldehyde bis(oxaloyldihydrazone). *Spectrochim. Acta Part A* 140, 344–355.
- Rawat, P., Singh, R.N., 2015b. Synthesis, conformational, spectroscopic and chemical reactivity analysis of 2-cyano-3-(1H-pyrrol-2-yl)acryloylhydrazone using experimental and quantum chemical approaches. *J. Mol. Struct.* 1082, 118–130.
- Rawat, P., Singh, R.N., 2019. Synthesis, spectral analysis and study of antimicrobial activity of 2,5-diformyl-1H-pyrrole bis(methan-1-yl-1-ylidene)dimalonohydrazone. *Arab. J. Chem.* 12, 1219–1233, <http://dx.doi.org/10.1016/j.arabj.2014.10.050>.
- Richardson, D.R., Bernhardt, P.V., 1999. Crystal and molecular structure of 2-hydroxy-1-naphthaldehyde isonicotinoyl hydrazone (NIH) and its iron(III) complex: an iron chelator with antitumor. *Biol. Inorg. Chem.* 4, 266–273.
- Rollas, S., Kükükgüzel, S.G., 2007. *Biol. Activ. Hydraz. Derivat. Molec.* 12, 1910–1939.
- Savini, L., Chiasserini, L., Travagli, V., Pellerano, C., Novellino, E., Cosentino, S., Pisano, M.B., 2004. New  $\alpha$ -(N)-heterocyclic hydrazones: evaluation of anticancer, anti-HIV and antimicrobial activity. *Eur. J. Med. Chem.* 39, 113–122.
- Shirota, Y., Kageyama, H., 2007. Charge carrier transporting molecular materials and their applications in devices. *Chem. Rev.* 107, 953–1010.
- Silverstein, R.M., Webster, F.X., 1963. *Spectrometric Identification of Organic Compounds*, sixth ed. Jon Wiley Sons, Inc., New York.
- Singh, R.N., Rawat, P., 2013. Spectral analysis, structural elucidation, and evaluation of both nonlinear optical properties and chemical reactivity of a newly synthesized ethyl-3,5-dimethyl-4-[(toluenesulfonyl)-hydrazonomethyl]-1H-pyrrole-2-carboxylate through experimental studies and quantum chemical calculations. *J. Mol. Struct.* 1054–1055, 65–75.
- Singh, R.N., Kumar, A., Rawat, P., Srivastava, A., 2013a. Synthesis, spectroscopic and structural evaluation of ethyl 2-cyano-3-{5-[(4-nitro-benzoyl)-hydrazonomethyl]-1H-pyrrol-2-yl}-acrylate using experimental and theoretical approaches. *J. Mol. Struct.* 1049, 419–428.
- Singh, R.N., Rawat, P., Sahu, S., 2013b. Investigation of spectroscopic, structural and non-linear optical properties of ethyl 3, 5-

- dimethyl-4-[(benzenesulfonyl)-hydrazonoethyl]-1H-pyrrol-2-carboxylate. *J. Mol. Struct.* 1054, 123–133.
- Singh, R.N., Baboo, V., Rawat, P., Gupta, V.P., 2013c. Studies on molecular weaker interactions, spectroscopic analysis and chemical reactivity of synthesized ethyl 3,5-dimethyl-4-[3-(2-nitro-phenyl)-acryloyl]-1H-pyrrole-2-carboxylate through experimental and quantum chemical approaches. *J. Mol. Struct.* 1037, 338–351.
- Singh, R.N., Kumar, A., Tiwari, R.K., Rawat, P., Manohar, R., 2013d. Synthesis, molecular structure, and spectral analyses of ethyl-4-[(2, 4-dinitrophenyl)-hydrazonomethyl]-3, 5-dimethyl-1H-pyrrole-2-carboxylate. *Struct. Chem.* 24, 713–724.
- Singh, R.N., Kumar, A., Tiwari, R.K., Rawat, P., Gupta, V.P., 2013e. A combined experimental and quantum chemical (DFT and AIM) study on molecular structure, spectroscopic properties, NBO and multiple interaction analysis in a novel ethyl 4-[2-(carbamoyl)hydrazinylidene]-3,5-dimethyl-1H-pyrrole-2-carboxylate and its dimer. *J. Mol. Struct.* 1035, 427–440.
- Singh, R.N., Kumar, A., Tiwari, R.K., Rawat, P., 2014a. Synthesis, molecular structure, multiple interactions and chemical reactivity analysis of a novel ethyl 2-cyano-3-[5-(hydrazinooxalyl)-hydrazonomethyl]-1H-pyrrol-2-yl]-acrylate and its dimer: A combined experimental and theoretical (DFT and QTAIM) approach. *J. Mol. Struct.* 1037, 420–430.
- Singh, R.N., Rawat, P., Kumar, A., 2014b. Synthesis, molecular structure, photoluminescence, multiple interaction, chemical reactivity and first hyperpolarizability analysis of Ethyl 2-cyano-3-[5-(4-methylbenzenesulfonyl)-hydrazonomethyl]-1H-pyrrol-2-yl]-acrylate: experimental and quantum chemical approaches. *J. Mol. Struct.* 1061, 140–149.
- Sour, A., Boillot, M.L., Riviere, E., Lesot, P., 1999. First evidence of a photoinduced spin change in an Fe(III) complex using visible light at room temperature. *Eur. J. Inorg. Chem.* 1999, 2117–2119.
- Szczesna, B., Lipkowska, U., 2001. Solid-to-solid reaction of 2,4-dinitrophenylhydrazine with several aromatic aldehydes bearing electron-donating groups. *Supramol. Chem.* 13, 247–251.
- Tang, B., Zhang, L., Zhang, J., Chen, Z., Wang, Y., 2004. Synthesis of a novel host molecule of cross-linking-polymeric- $\beta$ -cyclodextrin-*o*-vanillin furfuralhydrazone and spectrofluorimetric analysis of its identifying cadmium. *Spectrochim. Acta Part A* 60, 2425–2431.
- Uniyal, N., Sharma, M., Sharma, B., Tripathi, R.B., 2010. Quantifying the charge transfer phenomenon by molar refractivity in binding of 4-quinoinyl derivatives as antimalarials. *Int. J. Chem. Tech. Res.* 2, 1468–1472.
- Verma, R.P., Hansch, C., 2005. A comparison between two polarizability parameters in chemical–biological interactions. *Bioorg. Med. Chem.* 13, 2355–2372.
- Vijayakumar, S., Adithya, A., Sharafudeen, K.N., Balakrishna, K., Chandrasekharan, K., 2010. Third-order nonlinear optical properties in 4-[(E)-(2-phenylhydrazinylidene)methyl]tetrazolo[1,5-a]quinoline doped PMMA thin film using Z-scan technique. *J. Mod. Optic* 57, 670–676.
- Vijayakumar, S., Adhikari, A., Kalluraya, B., Sharafudeen, K.N., Chandrasekharan, K., 2011. Study of third-order optical nonlinearities of substituted hydrazones in PMMA. *J. Appl. Polym. Sci.* 119, 595–601.
- Vogel, A.I., 1956. *Textbook of Practical Organic Chemistry*, third ed. Prentice Hall, John Wiley & Sons, Inc., New York.
- Vogt, R.F., Martin, G.E., Zenger, V., 2008. In: Wolfbeis, O.S. (Ed.), *Springer Series on Fluorescence*. Springer, Berlin, pp. 4–31.
- Wei, E.-Y., 2012. (E)-N'-(5-Bromo-2-hydroxy-benzylidene)-4-(dimethyl-amino) benzohydrazide. *Acta Cryst. E* 68, o1304.
- Wild, E.F., 1947. Characterization of organic compounds. *J. Phys. Chem.* 51, 1450–1450.
- Wolinski, K., Hinton, J.F., Pulay, J.F., 1990. Efficient implementation of the gauge-independent atomic orbital method for NMR chemical shift calculations. *J. Am. Chem. Soc.* 112, 8251–8260.
- Yu, M., Lin, H., Lin, H., 2007. Synthesis and anion recognition of acetate ions using pyrrole- $\alpha$ -carboxaldehyde 2, 4-dinitrophenyl hydrazine. *Ind. J. Chem. Sec A* 46, 1437–1439.
- Zheng, L.W., Wu, L.L., Zhao, B.X., Dong, W.L., Miao, Y.J., 2009. Synthesis of novel substituted pyrazole-5-carbohydrazidehydrazone derivatives and discovery of a potent apoptosis inducer in A549 lung cancer cells. *Bioorg. Med. Chem.* 17, 1957–1962.
- Zong, Q.-S., 2012. N'-(3-Fluorobenzylidene)-4-hydroxy-3-methoxy-benzohydrazide methanol monosolvate. *Acta Cryst. E* 68, o1338.